nanomaterials

MDPI

Article

Effects of Electrolyte on Laser-Induced Periodic Surface Structures with Picosecond Laser Pulses

Shuhei Kodama * and Wataru Natsu

Department of Mechanical Engineering, Tokyo University of Agriculture and Technology, 2-24-16 Nakacho, Koganei, Tokyo 184-8588, Japan; summer@cc.tuat.ac.jp

* Correspondence: shuhei-kodama@go.tuat.ac.jp; Tel.: +81-42-388-7776

Abstract: Short-pulsed laser-induced periodic surface structures (SPLIPSSs) have the possibility to control tribology, wettability and biocompatibility. Nevertheless, the optimal structure depends on each functionality, which has not been clarified. The hybrid process with a short-pulsed laser and electrochemical machining (SPLECM) is, then, proposed to fabricate micro/nano hybrid structures and to modify the surface composition for providing high functionalities with material surfaces. Electrochemical machining is a well-established micro-elution and deposition method with noncontact between a workpiece and a tool. In this study, the effects of electrolytes on SPLIPSSs were investigated experimentally by the picosecond laser irradiation on 304 stainless steel substrates in various electrolytes. The geometry of SPLIPSSs depended on the types and the concentration of electrolytes. In the case of copper nitrate solution and copper sulfate solution, LIPSSs and spheroidization of copper were obtained. This study demonstrated the possibility of SPLECM to fabricate micro/nano structures and to control surface composition.

Keywords: short-pulsed laser; laser-induced periodic surface structures (LIPSSs); electrochemical machining (ECM); electrolyte; nanostructure formation

Citation: Kodama, S.; Natsu, W. Effects of Electrolyte on Laser-Induced Periodic Surface Structures with Picosecond Laser Pulses. *Nanomaterials* **2021**, *11*, 327. https://doi.org/10.3390/nano11020327

Academic Editor: Aleksandr Kuchmizhak

Received: 24 December 2020

Accepted: 25 January 2021

Published: 27 January 2021

1. Introduction

Micro/Nanostructures can alter tribology [1,2], wettability [3,4], optical properties [5,6] and bioaffinity [7,8] on the material surface. The short-pulsed laser (SPL) is an appropriate method to fabricate nanostructures, called laser-induced periodic surface structures (LIPSSs), inducing a reduction of friction [9,10], water repellency and hydrophilicity [11–13], anti-reflection [14,15] and improvement of biocompatibility [16,17]. LIPSSs with a periodicity of 0.5–0.85 times the laser wavelength are fabricated through the self-organizing way [18]. The plasma waves, induced via protrusions on a surface based on the parametric decay [18–21], induced surface plasmons by the interference with the incident light, resulting in periodic Coulomb explosions [22] and ablation. Nevertheless, the appropriate structure for each functionality has not been clarified, although it has been reported that fine structures are effective to alter the surface reaction. In addition, fabrication of multiscale structures has been recently required to provide high added value with materials.

The hybrid manufacturing process is then proposed that combines an SPL and electrochemical machining (ECM), a noncontact machining method with electrolytic elution and deposition [23,24], to fabricate multiscale structures effectively and to control surface composition, in contrast to the laser-assisted electrochemical machining that combines a long-pulsed laser and ECM to increase the efficiency of ECM by enhancing thermal electrochemical action and removing the passive film [25–30].

The objectives of this study were to verify the effects of electrolytes on the fabrication of LIPSSs since a few studies have reported that LIPSS geometry depends on the irradiation environment [31]. We also aimed to spheroidize copper since ECM can coat with copper using copper nitrate ($Cu(NO_3)_2$) solution and copper sulfate ($CuSO_4$) solution [32–35] since

a long-pulsed laser or a continuous laser have been mainly used for laser enhanced electroless plating and the effects of an SPL on metal deposition with the fabrication of LIPSSs have never been studied. Experiments of laser irradiation with 1064 nm and 20 ps laser pulses at 0.04–1.0 J/cm^2 on the workpiece of 304 stainless steel under air, water, sodium chloride (NaCl) solution, sodium nitrate ($NaNO_3$) solution, copper nitrate ($Cu(NO_3)_2$) solution and copper sulfate ($CuSO_4$) solution, were conducted to fabricate LIPSSs in liquids and to change the surface composition. The spot size was 260 μm. In liquids, LIPSSs with less periodicity than LIPSSs under air were fabricated, and spheroidization of copper was obtained in $Cu(NO_3)_2$ solution and $CuSO_4$ solution. This paper describes the formation of LIPSSs in various electrolytes and the effects of short-pulsed laser irradiation in electrolytes on the surface composition.

2. Experiment

A 304 stainless steel plate (10 mm × 10 mm × 1.5 mm thickness) was used as a workpiece for this study to fabricate LIPSSs in various liquids. As liquids, we prepared water, 5 and 10 wt% NaCl solutions, 5 and 10 wt% $NaNO_3$ solutions, 5 and 10 wt% $Cu(NO_3)_2$ solutions and 5 and 10 wt% $CuSO_4$ solutions. NaCl solution and $NaNO_3$ solution are often used for ECM [23,24,36,37], and $Cu(NO_3)_2$ solution and $CuSO_4$ solution are used for electrochemical deposition of copper [32–35].

Short-pulsed laser irradiation experiments on a 304 stainless steel plate under air, water and electrolytes were conducted with a picosecond-pulse laser oscillator (EKXPLA, PL 2250-50P20) with 20 ps pulse duration. A longer pulse duration laser has a lower cost and more stable laser irradiation, and 20 ps is the approximate maximum of the collisional relaxation time of metals which is a key for the fabrication of LIPSSs.

Figure 1 shows the schematic diagram of the experimental setup including a half-wave plate to change the polarization state and to adjust laser power, a polarizer to isolate the specific polarization of light and a collecting lens with a focusing range of 150 mm. The workpiece was set in a quartz cell and set vertically to the ground. A workpiece was irradiated by a Gaussian laser beam on the fixed point without scanning. A picosecond Nd:YAG laser with a pulse duration of 20 ps, a wavelength of 1064 nm and a frequency of 50 Hz was used. The number of pulses N was set to 1–1000. The laser fluence F was set to 0.04–1.00 J/cm^2 by using a pair of a half-wave plate and a polarizer. The entire laser power was measured via the laser power meter, and the accurate beam profile was calculated by calibrating the measured beam profile via a charge-coupled device (CCD) beam profiler.

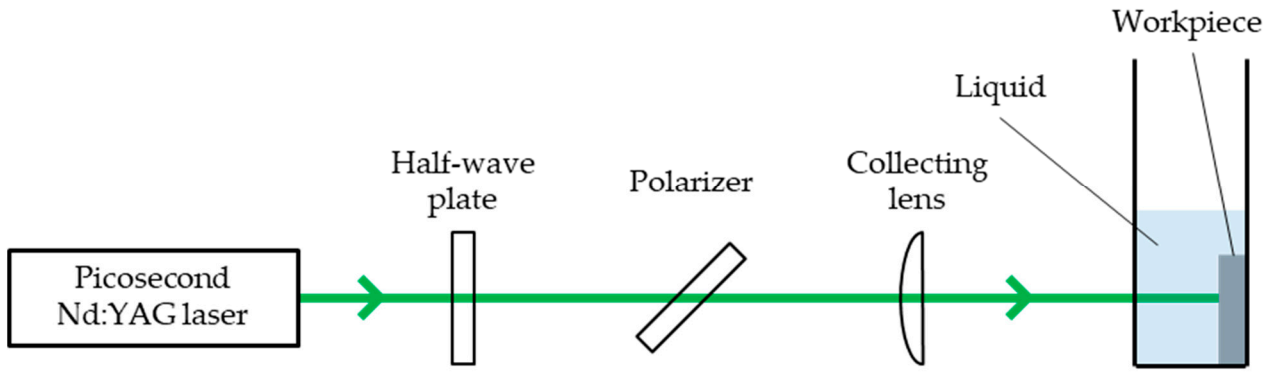

Figure 1. Schematic diagram of the experimental setup for laser irradiation on the material surface set vertically to the ground.

The surface morphology of the central irradiated area was observed using a scanning electron microscope (SEM, XL30, Philips, Eindhoven, The Netherlands). The surface geometries were further analyzed using a laser microscope (VK-X100, KEYENCE, Osaka, Japan) and an atomic force microscope (AFM, MultiMode 8, Bruker AXS, Karlsruhe, Germany). The periodicity of the LIPSSs was evaluated by a two-dimensional Fourier

transform performed on the SEM image along the polarization direction. The elemental analysis was conducted by the energy dispersive X-ray spectroscopy (EDX, EDAX DX-4, Philips, Eindhoven, The Netherlands).

3. Results and Discussion

Figures 2 and 3 show the SEM images of 304 stainless steel irradiated at $F = 0.04$–0.27 J/cm^2 for $N = 50$–1000 pulses under air and water, respectively. These demonstrate that LIPSSs perpendicular to the laser polarization were fabricated on the irradiated surface under air and water; on the other hand, LIPSSs with lower periodicity were fabricated in water when the low laser fluence compared to LIPSSs fabricated under air since large ablation on the irradiated surface causes disappearance of LIPSSs due to suppression of plasma expansion by water [38–41]. Figures 4 and 5 show the SEM images of 304 stainless steel irradiated at $F = 0.04$–0.08 J/cm^2 for $N = 50$–1000 pulses in 5 and 10 wt% NaCl solutions and 5 and 10 wt% $NaNO_3$ solutions, respectively. These demonstrate that LIPSSs with lower periodicity were fabricated at lower laser fluence in both solutions than LIPSSs fabricated under air, similar to LIPSSs fabricated in water. Figures 6 and 7 show the SEM images of 304 stainless steel irradiated at $F = 0.04$–0.45 J/cm^2 for $N = 50$–1000 pulses in 5 and 10 wt% $Cu(NO_3)_2$ solutions and 5 and 10 wt% $CuSO_4$ solutions, respectively. These demonstrate that LIPSSs with lower periodicity were fabricated at a wide-range laser fluence in both solutions, and copper particles were deposited on the irradiated surface and grew with increasing the number of pulses since plasma generation reduced the copper ion in the solutions to form copper particles on the irradiated surface and made these grow [42–44].

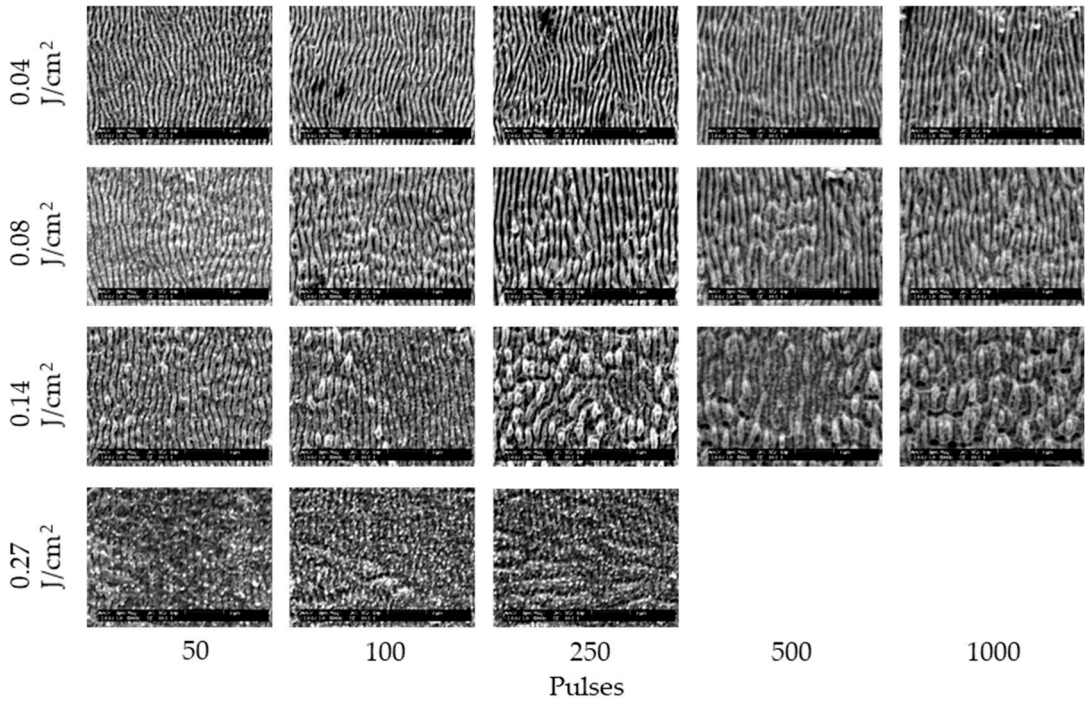

Figure 2. SEM images of 304 stainless steel irradiated with $N = 50$–1000 pulses at $F = 0.04$–0.27 J/cm^2 under air. The laser beam has the polarization in a lateral direction.

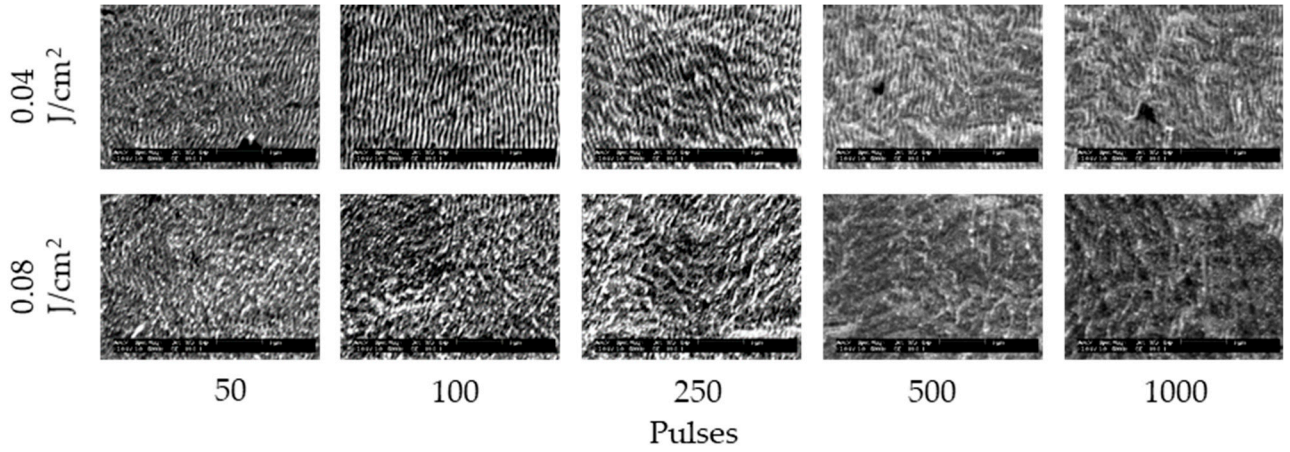

Figure 3. SEM images of 304 stainless steel irradiated with N = 50–1000 pulses at F = 0.04–0.08 J/cm^2 in water. The laser beam has the polarization in a lateral direction.

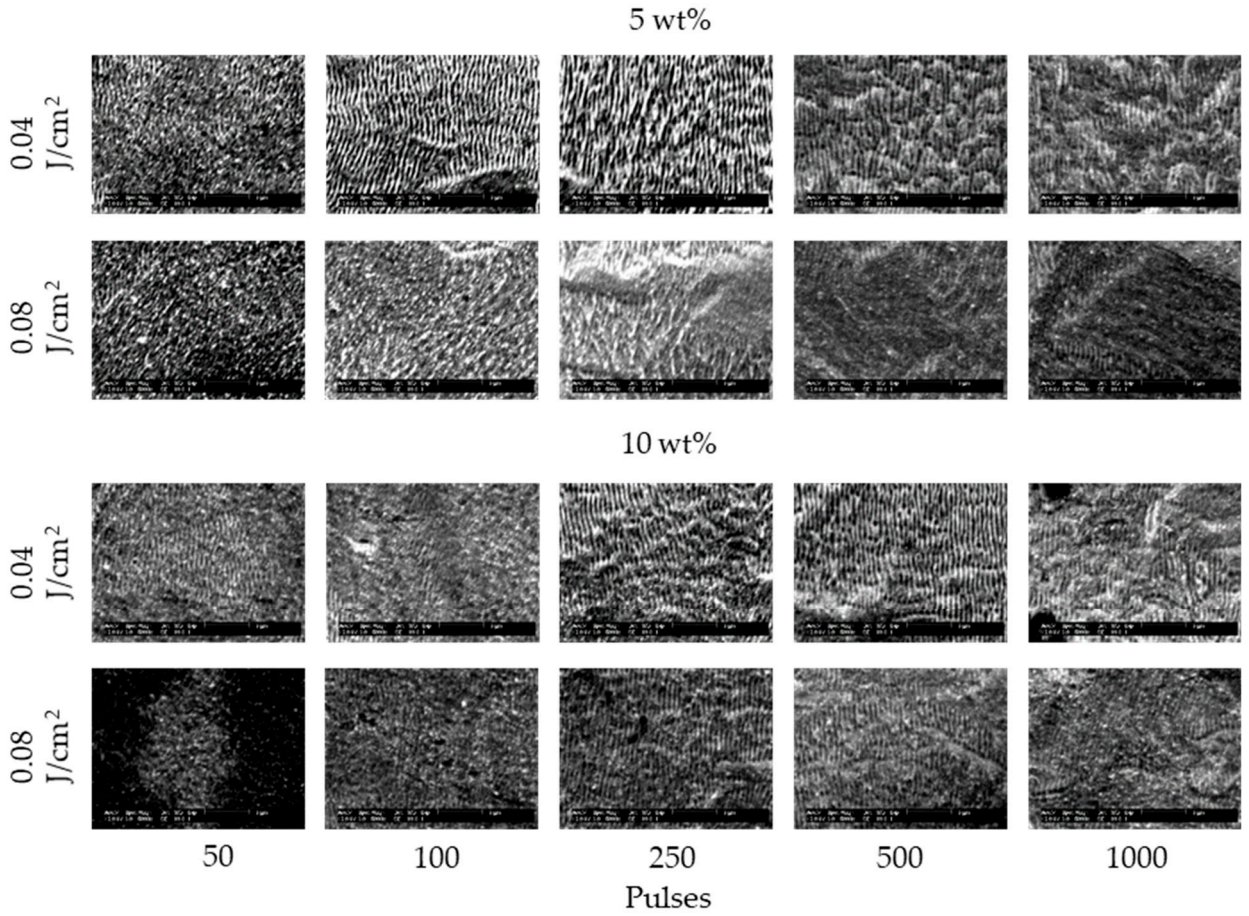

Figure 4. SEM images of 304 stainless steel irradiated with N = 50–1000 pulses at F = 0.04–0.08 J/cm^2 in 5 and 10 wt% NaCl solutions. The laser beam has the polarization in a lateral direction.

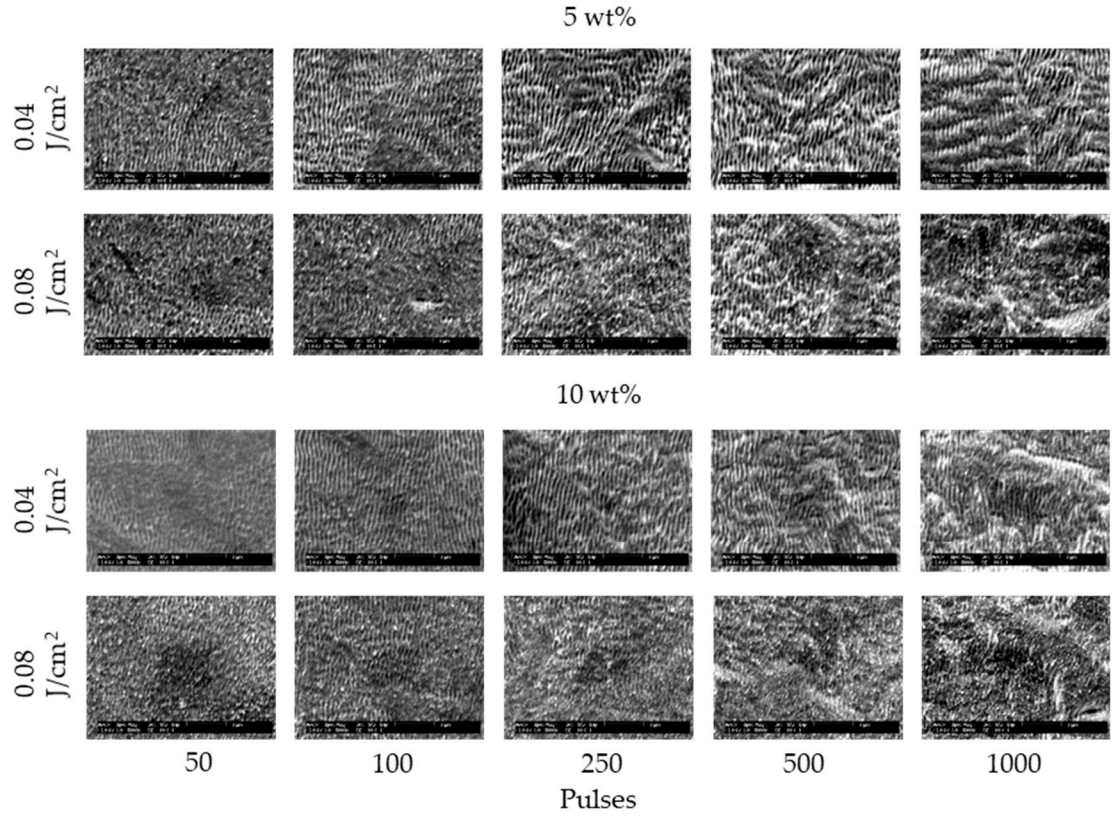

Figure 5. SEM images of 304 stainless steel irradiated with N = 50–1000 pulses at F = 0.04–0.08 J/cm^2 in 5 and 10 wt% $NaNO_3$ solutions. The laser beam has the polarization in a lateral direction.

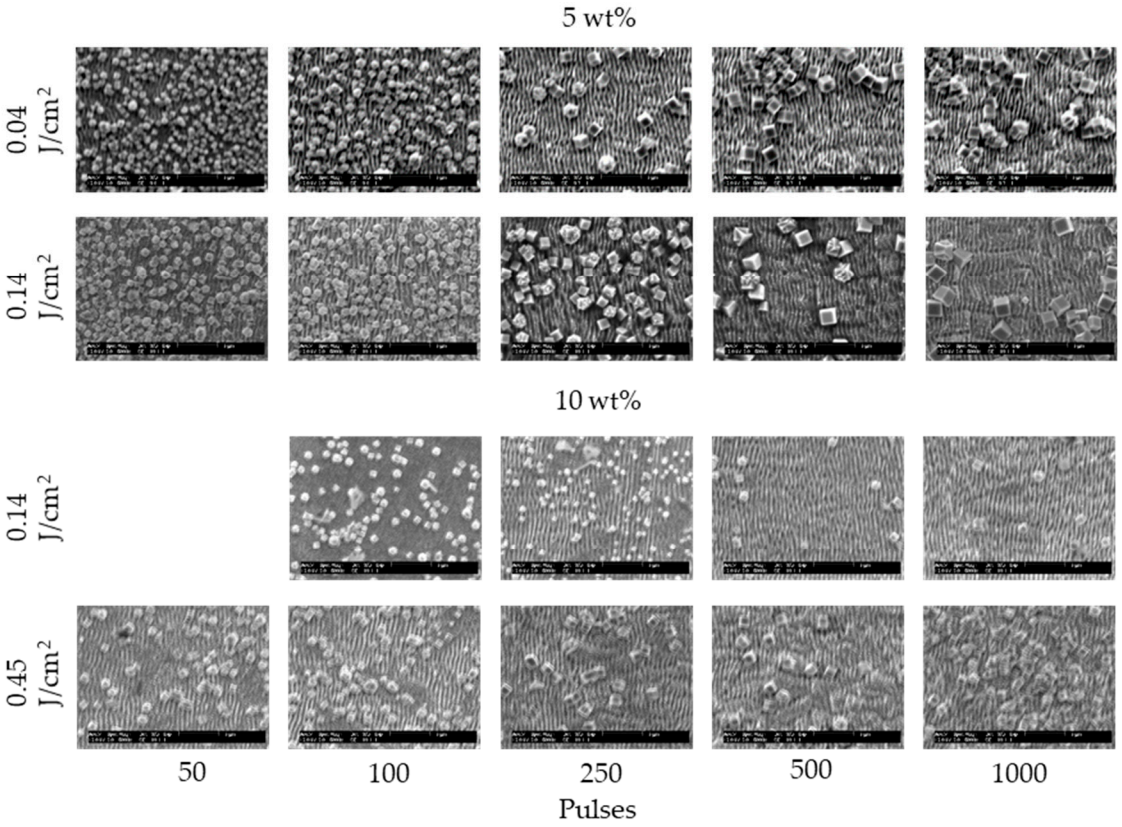

Figure 6. SEM images of 304 stainless steel irradiated with N = 50–1000 pulses at F = 0.04–0.45 J/cm^2 in 5 and 10 wt% $Cu(NO_3)_2$ solutions. The laser beam has the polarization in a lateral direction.

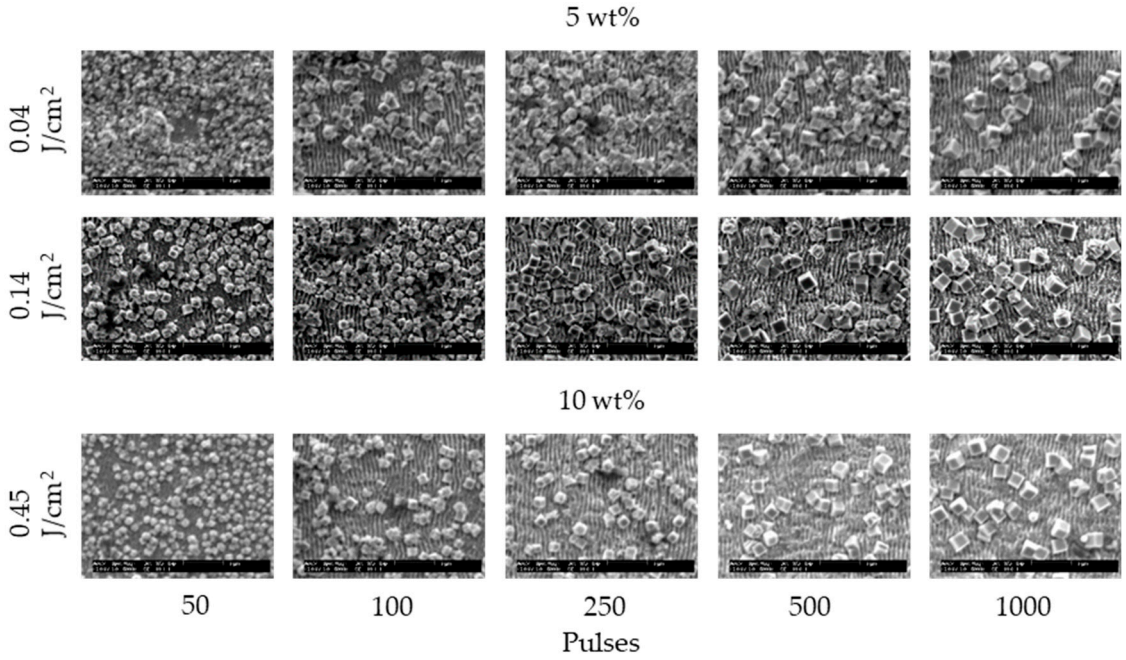

Figure 7. SEM images of 304 stainless steel irradiated with N = 50–1000 pulses at F = 0.04–0.45 J/cm^2 in 5 and 10 wt% $CuSO_4$ solutions. The laser beam has the polarization in a lateral direction.

Figure 8 shows changes in the periodicity of LIPSSs fabricated on 304 stainless steel surfaces under air, water, 5 and 10 wt% NaCl solutions, 5 and 10 wt% $NaNO_3$ solutions, 5 and 10 wt% $Cu(NO_3)_2$ solutions and 5 and 10 wt% $CuSO_4$ solutions for each irradiation condition. The periodicity of LIPSSs on the 304 stainless steel surfaces under air was about 700–900 nm, which was about 0.65–0.85 times the laser wavelength. This phenomenon was attributed to the surface plasma waves whose wavelength is 0.50–0.85 times the laser wavelength, and the increase of the electron density extends it, explained by the parametric decay [18–21]. On the other hand, the periodicity of LIPSSs on the 304 stainless steel surfaces in water, 5 and 10 wt% NaCl solutions, 5 and 10 wt% $NaNO_3$ solutions, 5 and 10 wt% $Cu(NO_3)_2$ solutions and 5 and 10 wt% $CuSO_4$ solutions was about 600 nm, which was about 0.56 times the laser wavelength since the refractive index of water is 1.33 [45], shortening the laser wavelength and the wavelength of the surface plasma waves. In the solutions, the periodicity is approximately the same since the refractive index of 5 and 10 wt% NaCl solutions, 5 and 10 wt% $NaNO_3$ solutions, 5 and 10 wt% $Cu(NO_3)_2$ solutions and 5 and 10 wt% $CuSO_4$ solutions is close to the refractive index of water [46–50].

Figure 9 shows the changes in height of LIPSSs fabricated on 304 stainless steel surfaces under air, water, 5 and 10 wt% NaCl solutions, 5 and 10 wt% $NaNO_3$ solutions, 5 and 10 wt% $Cu(NO_3)_2$ solutions and 5 and 10 wt% $CuSO_4$ solutions for each irradiation condition. The LIPSS height in solutions was 150–300 nm, which was lower than the LIPSS height of 300–500 nm under air [51]. This can be attributed to the attenuation of light in solutions decreasing the intensity of the plasma waves and the suppression of plasma expansion removing LIPSSs [38–41]. With the increase of the number of pulses and fluence, the height of LIPSSs increased gradually under air, water, NaCl solutions and NaNO3 solutions, however, the height of LIPSSs in $Cu(NO_3)_2$ solution and $CuSO_4$ solution was not proportional to the number of pulses since deposited copper particles which grew and were removed with the increasing number of pulses changed induction and propagation of the plasma waves. In solutions, the height of LIPSSs in $Cu(NO_3)_2$ solution and $CuSO_4$ solution was larger than that in other solutions since the deposited copper particles facilitate the induction and propagation of the plasma waves, increasing the electric field intensity on the surface.

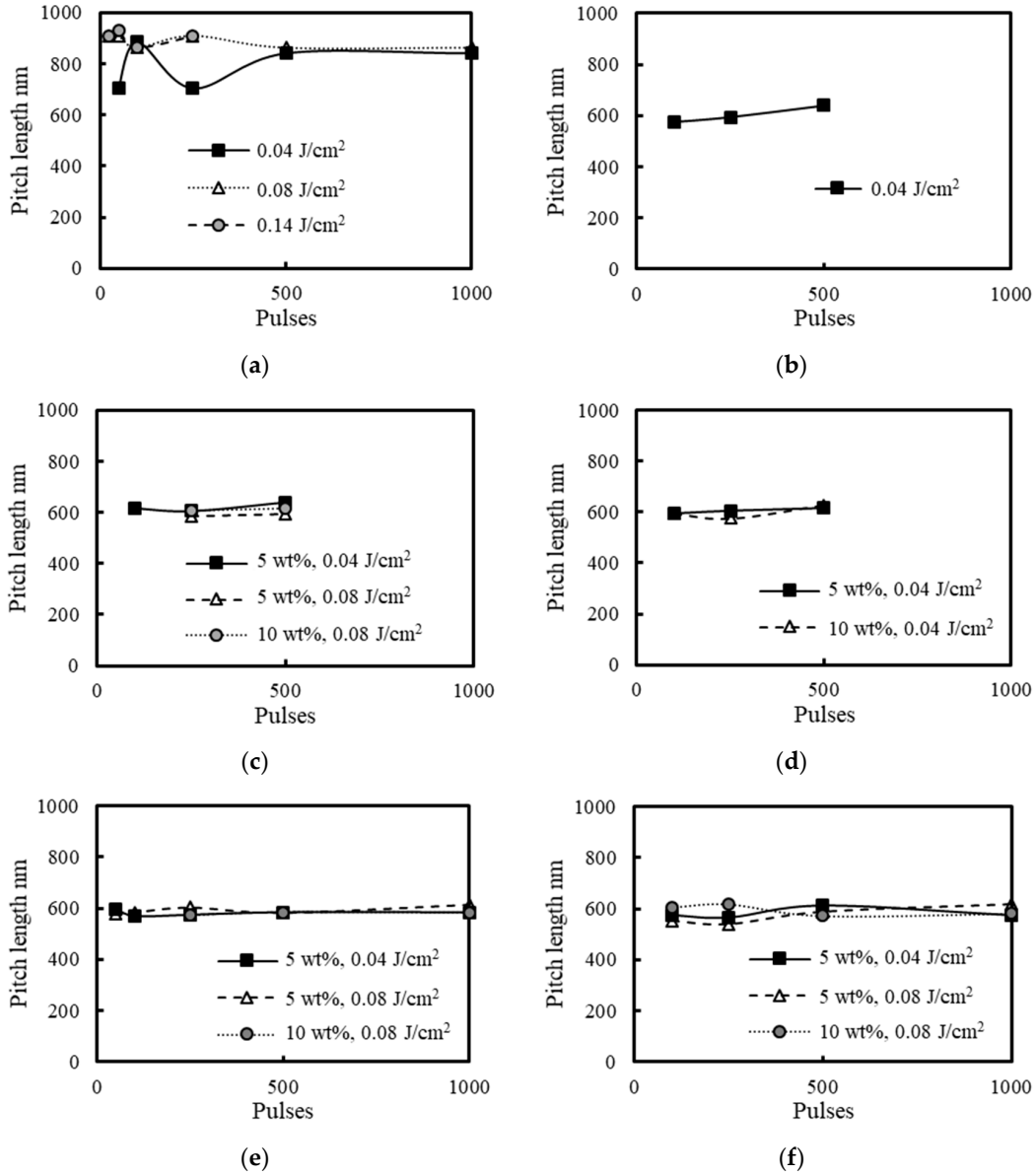

Figure 8. Relationship between the periodicity of laser-induced periodic surface structures (LIPSSs) and laser irradiation conditions under (**a**) air, (**b**) water, (**c**) 5 and 10 wt% NaCl solutions, (**d**) 5 and 10 wt% $NaNO_3$ solutions, (**e**) 5 and 10 wt% $Cu(NO_3)_2$ solutions and (**f**) 5 and 10 wt% $CuSO_4$ solutions.

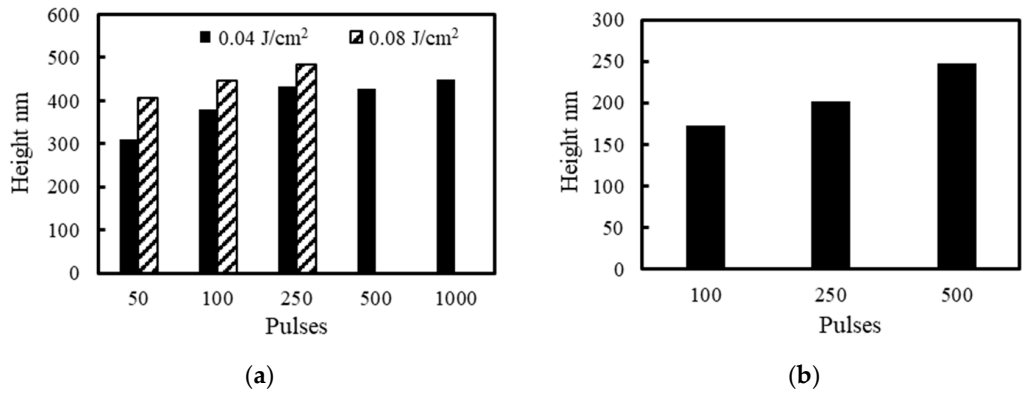

Figure 9. *Cont.*

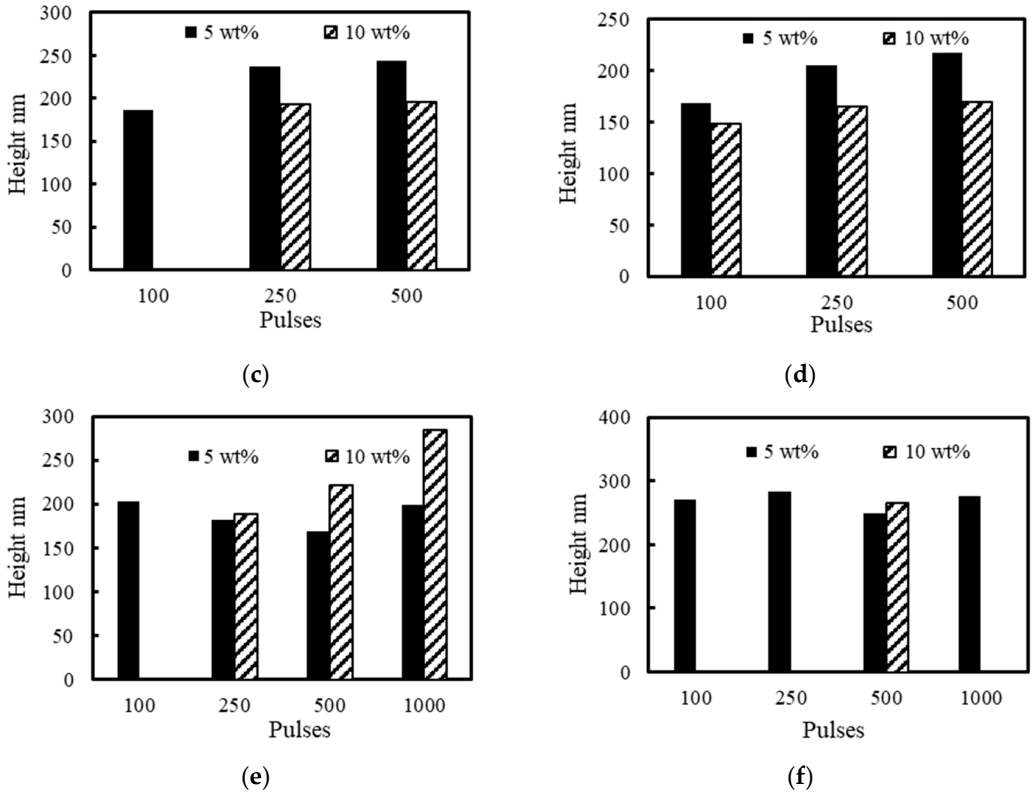

Figure 9. Relationship between the height of LIPSSs and laser irradiation conditions under (**a**) air, (**b**) water, (**c**) 5 and 10 wt% NaCl solutions, (**d**) 5 and 10 wt% $NaNO_3$ solutions, (**e**) 5 and 10 wt% $Cu(NO_3)_2$ solutions and (**f**) 5 and 10 wt% $CuSO_4$ solutions.

The depth of craters was measured by a laser microscope as shown in Figure 10. Figure 11 shows the depth of craters on 304 stainless steel surfaces with N = 500 pulses at F = 0.04 J/cm^2 under air, water, 5 wt% NaCl solution, 5 wt% $NaNO_3$ solution, 5 wt% $Cu(NO_3)_2$ solution and 5 wt% $CuSO_4$ solution. The depth of craters in the solutions was larger than that under air since solutions suppressed the plasma expansion and induced large ablation [38–41]. In solutions, the depth of craters in NaCl solution was larger than that in other solutions due to low attenuation [25].

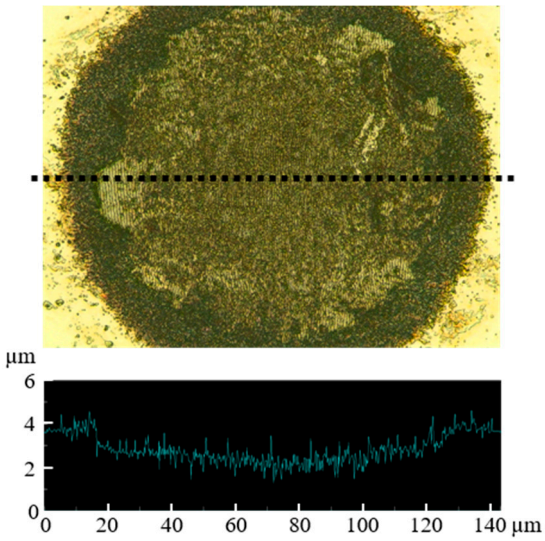

Figure 10. Topography of craters with N = 500 pulses at F = 0.04 J/cm^2 under air.

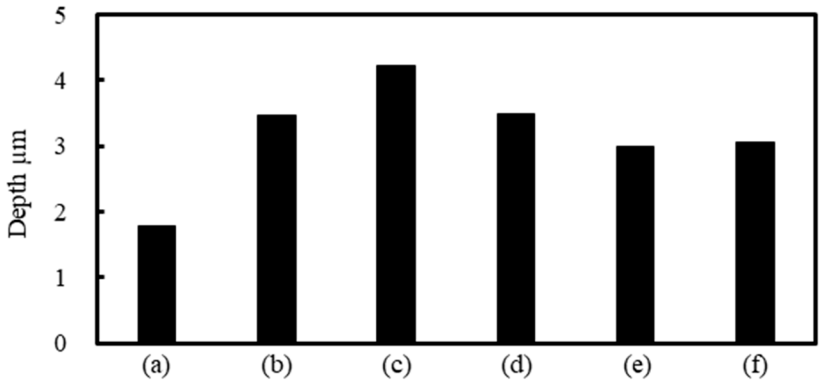

Figure 11. Relationship between the depth of craters and laser irradiation conditions with N = 500 pulses at F = 0.04 J/cm^2 under (**a**) air, (**b**) water, (**c**) 5 wt% NaCl solution, (**d**) 5 wt% $NaNO_3$ solution, (**e**) 5 wt% $Cu(NO_3)_2$ solution and (**f**) 5 wt% $CuSO_4$ solution.

Figure 12 shows the elements of surfaces of non-irradiated and irradiated areas with N = 500 pulses at F = 0.04 J/cm^2 under air, water, 5 wt% NaCl solution, 5 wt% $NaNO_3$ solution, 5 wt% $Cu(NO_3)_2$ solution and 5 wt% $CuSO_4$ solution. The elements of surfaces were almost the same under air, water, NaCl solution and $NaNO_3$ solution; on the other hand, the surfaces in $Cu(NO_3)_2$ solution and $CuSO_4$ solution had the copper element, meaning that copper particles were deposited on the surfaces by laser irradiation in $Cu(NO_3)_2$ solution and $CuSO_4$ solution [42–44]. The composition of copper deposition of $CuSO_4$ was larger than $Cu(NO_3)_2$. It is considered that the lower attenuation of the laser causes more copper deposition in $CuSO_4$ solution due to $Cu(NO_3)_2$ of a larger molecular weight scattering a laser beam, leading to high LIPSSs and deep craters in $CuSO_4$ solution.

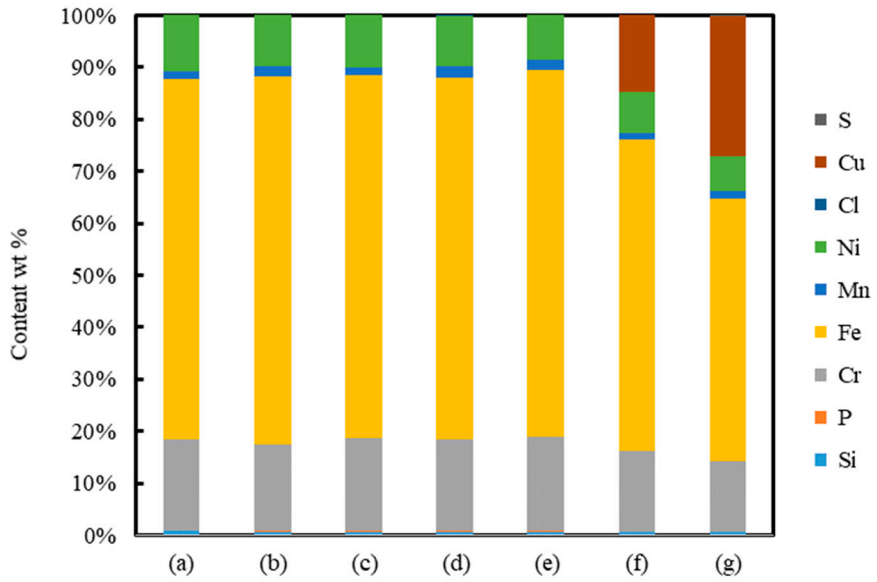

Figure 12. Relationship between elements of surfaces of (**a**) non-irradiated area and irradiated areas with N = 500 pulses at F = 0.04 J/cm^2 under (**b**) air, (**c**) water, (**d**) 5 wt% NaCl solution, (**e**) 5 wt% $NaNO_3$ solution, (**f**) 5 wt% $Cu(NO_3)_2$ solution and (**g**) 5 wt% $CuSO_4$ solution.

4. Conclusions

LIPSSs were fabricated on the 304 stainless steel surface by using a 20 ps laser in water, NaCl solution, $NaNO_3$ solution, $Cu(NO_3)_2$ solution and $CuSO_4$ solution at low fluence. In the case of $Cu(NO_3)_2$ solution and $CuSO_4$ solution, copper particles were deposited on the irradiated surfaces analyzed by EDX. The periodicity of LIPSSs in solutions was about 600 nm, which was shorter than that under air due to the refractive index shortening

the laser wavelength. The LIPSS height of 150–300 nm in solutions was lower than that under air due to the attenuation of light; on the other hand, the depth of craters in the solutions was larger than that under air due to the suppression of plasma expansion and large ablation. The 20 ps laser irradiation in solutions can fabricate LIPSSs with shorter periodicity, depositing copper particles.

Author Contributions: Conceptualization, S.K. and W.N.; methodology, S.K. and W.N.; software, S.K.; validation, S.K.; formal analysis, S.K.; investigation, S.K.; resources, S.K.; data curation, S.K.; writing—original draft preparation, S.K.; writing—review and editing, S.K. and W.N.; visualization, S.K. and W.N.; supervision, S.K. and W.N.; project administration, S.K. and W.N.; funding acquisition, S.K. All authors have read and agreed to the published version of the manuscript.

Funding: This research was partially supported by the Grant-in-Aid for Early-Career Scientists (20K14620).

Acknowledgments: The authors would like to thank T. Kuriyagawa and M. Mizutani for performing the experiment.

Conflicts of Interest: The authors declare no conflict of interest. The funders had no role in the design of the study; in the collection, analyses, or interpretation of data; in the writing of the manuscript, or in the decision to publish the results.

References

1. Kim, E.S.; Kim, S.M.; Lee, Y.Z. The effect of plateau honing on the friction and wear of cylinder liners. *Wear* **2018**, *400*, 207–212. [CrossRef]
2. Ji, M.; Xu, J.; Chen, M.; El Mansori, M. Enhanced hydrophilicity and tribological behavior of dental zirconia ceramics based on picosecond laser surface texturing. *Ceram. Int.* **2020**, *46*, 7161–7169. [CrossRef]
3. Shamsudin, S.; Ahmad, M.K.; Aziz, A.N.; Fakhriah, R.; Mohamad, F.; Ahmad, N.; Nafarizal, N.; Soon, C.F.; Ameruddin, A.S.; Faridah2, A.B.; et al. Hydrophobic rutile phase TiO_2 nanostructure and its properties for self-cleaning application. *AIP Conf. Proc.* **2017**, *1883*, 1–9.
4. Wang, H.; Zhuang, J.; Yu, J.; Qi, H.; Ma, Y.; Wang, H.; Guo, Z. Fabrication of Anti-Reflective Surface with Superhydrophobicity/High Oleophobicity and Enhanced Mechanical Durability via Nanosecond Laser Surface Texturing. *Materials* **2020**, *13*, 5691. [CrossRef] [PubMed]
5. Chen, T.; Wang, W.; Tao, T.; Pan, A.; Mei, X. Multi-scale micro-nano structures prepared by laser cleaning assisted laser ablation for broadband ultralow reflectivity silicon surfaces in ambient air. *Appl. Surf. Sci.* **2020**, *509*, 145182. [CrossRef]
6. Samanta, A.; Wang, Q.; Singh, G.; Shaw, S.K.; Toor, F.; Ratner, A.; Ding, H. Nanosecond pulsed laser processing turns engineering metal alloys antireflective and superwicking. *J. Manuf. Process.* **2020**, *54*, 28–37. [CrossRef]
7. Elena Sima, L.; Bonciu, A.; Baciu, M.; Anghel, I.; Dumitrescu, L.N.; Rusen, L.; Dinca, V. Bioinstructive Micro-Nanotextured Zirconia Ceramic Interfaces for Guiding and Stimulating an Osteogenic Response In Vitro. *Nanomaterials* **2020**, *10*, 2465. [CrossRef]
8. Pawar, D.R.L.; Jeyapalina, S.; Bachus, K.N. Evaluation of soft-tissue response around laser microgrooved titanium percutaneous devices. *J. Biomed. Mater. Res. Part B Appl. Biomater.* **2020**, *108*, 2031–2040. [CrossRef]
9. Gnilitskyi, I.; Rota, A.; Gualtieri, E.; Valeri, S.; Orazi, L. Tribological Properties of High-Speed Uniform Femtosecond Laser Patterning on Stainless Steel. *Lubricants* **2019**, *7*, 83. [CrossRef]
10. Murzin, S.P.; Balyakin, V.B.; Liedl, G.; Melnikov, A.A.; Fürbacher, R. Improving Tribological Properties of Stainless Steel Surfaces by Femtosecond Laser Irradiation. *Coatings* **2020**, *10*, 606. [CrossRef]
11. Chu, D.K.; Yin, K.; Dong, X.R.; Luo, Z.; Duan, J.A. Femtosecond laser fabrication of robust underwater superoleophobic and anti-oil surface on sapphire. *Aip Adv.* **2017**, *7*, 8. [CrossRef]
12. Kobayashi, T.; Yan, J. Generating Nanodot Structures on Stainless-Steel Surfaces by Cross Scanning of a Picosecond Pulsed Laser. *Nanomanuf. Metrol.* **2020**, *3*, 105–111. [CrossRef]
13. Žemaitis, A.; Mimidis, A.; Papadopoulos, A.; Gečys, P.; Račiukaitis, G.; Stratakis, E.; Gedvilas, M. Controlling the wettability of stainless steel from highly-hydrophilic to super-hydrophobic by femtosecond laser-induced ripples and nanospikes. *RSC Adv.* **2020**, *10*, 37956–37961. [CrossRef]
14. Lee, K.; Ki, H. Femtosecond laser patterning based on the control of surface reflectance. *Appl. Surf. Sci.* **2019**, *494*, 187–195. [CrossRef]
15. Nigo, F.; Hashida, M.; Tsukamoto, M.; Sakabe, S.; Kusaba, M. Reflectance and crystallinity of silicon solar cells with LIPSS produced by XeCl excimer laser pulses. *Appl. Phys. A* **2020**, *126*, 129. [CrossRef]
16. Shinonaga, T.; Tsukamoto, M. Creation of New Functional Biomaterials by Periodic Nanostructures Formation with Femtosecond Laser. *J. Jpn Soc. Precis. Eng.* **2015**, *81*, 726–730. [CrossRef]

17. Luo, X.; Yao, S.; Zhang, H.; Cai, M.; Liu, W.; Pan, R.; Chen, C.; Wang, X.; Wang, L.; Zhong, M. Biocompatible nano-ripples structured surfaces induced by femtosecond laser to rebel bacterial colonization and biofilm formation. *Opt. Laser Technol.* **2020**, *124*, 105973. [CrossRef]
18. Okamuro, K.; Hashida, M.; Miyasaka, Y.; Ikuta, Y.; Tokita, S.; Sakabe, S. Laser fluence dependence of periodic grating structures formed on metal surfaces under femtosecond laser pulse irradiation. *Phys. Rev. B* **2010**, *82*, 165417. [CrossRef]
19. Maruo, S.; Nakamura, O.; Kawata, S. Evanescent-wave holography: By use of surface-plasmon resonance. *Appl. Opt.* **1997**, *36*, 2343–2346. [CrossRef]
20. Sakabe, S.; Hashida, M.; Tokita, S.; Namba, S.; Okamuro, K. Mechanism for self-formation of periodic grating structures on a metal surface by a femtosecond laser pulse. *Phys. Rev. B* **2009**, *79*, 4. [CrossRef]
21. Gemini, L.; Hashida, M.; Miyasaka, Y.; Inoue, S.; Limpouch, J.; Mocek, T.; Sakabe, S. Periodic surface structures on titanium self-organized upon double femtosecond pulse exposures. *Appl. Surf. Sci.* **2015**, *336*, 349–353. [CrossRef]
22. Kodama, S.; Yamaguchi, H.; Shimada, K.; Mizutani, M.; Kuriyagawa, T. Control of short-pulsed laser induced periodic surface structures with machining—Picosecond laser nanotexturing with magnetic abrasive finishing. *Precis. Eng. J. Int. Soc. Precis. Eng. Nanotechnol.* **2019**, *60*, 428–436. [CrossRef]
23. Wang, Y.; Xu, Z.; Zhang, A. Electrochemical dissolution behavior of Ti-45Al-2Mn-2Nb+0.8 vol% TiB_2 XD alloy in NaCl and $NaNO_3$ solutions. *Corros. Sci.* **2019**, *157*, 357–369. [CrossRef]
24. Ayyappan, S.; Sivakumar, K. Investigation of electrochemical machining characteristics of 20MnCr5 alloy steel using potassium dichromate mixed aqueous NaCl electrolyte and optimization of process parameters. *Proc. Inst. Mech. Eng. Part B J. Eng. Manuf.* **2015**, *229*, 1984–1996. [CrossRef]
25. Zhang, H.; Xu, J.W.; Wang, J.M. Investigation of a novel hybrid process of laser drilling assisted with jet electrochemical machining. *Opt. Lasers Eng.* **2009**, *47*, 1242–1249. [CrossRef]
26. Long, Y.H.; Shi, T.L.; Xiong, L.C. Excimer laser electrochemical etching n-Si in the KOH solution. *Opt. Lasers Eng.* **2010**, *48*, 570–574. [CrossRef]
27. De Silva, A.K.M.; Pajak, P.T.; McGeough, J.A.; Harrison, D.K. Thermal effects in laser assisted jet electrochemical machining. *Cirp Ann. Manuf. Technol.* **2011**, *60*, 243–246. [CrossRef]
28. Long, Y.H.; Li, Q.Y.; Zhong, Z.X.; Xiong, L.C.; Shi, T.L. Experimental study on the processes of laser-enhanced electrochemical micromachining stainless steel. *Optik* **2015**, *126*, 1826–1829. [CrossRef]
29. Duan, W.; Mei, X.; Fan, Z.; Li, J.; Wang, K.; Zhang, Y. Electrochemical corrosion assisted laser drilling of micro-hole without recast layer. *Optik* **2020**, *202*, 163577. [CrossRef]
30. Saxena, K.K.; Qian, J.; Reynaerts, D. A tool-based hybrid laser-electrochemical micromachining process: Experimental investigations and synergistic effects. *Int. J. Mach. Tools Manuf.* **2020**, *155*, 103569. [CrossRef]
31. Kobayashi, T.; Wakabayashi, T.; Takushima, Y.; Yan, J.W. Formation behavior of laser-induced periodic surface structures on stainless tool steel in various media. *Precis. Eng. J. Int. Soc. Precis. Eng. Nanotechnol.* **2019**, *57*, 244–252. [CrossRef]
32. Sallee, N.; Cromer, M.; Vittori, O. Electroplating of Copper on Aluminum with Direct and Pulsed Currents. *Can. Metall. Q.* **1994**, *33*, 155–162. [CrossRef]
33. Behera, A.K.; Mallik, A. Ultrasound assisted electroplating of nano-composite thin film of Cu matrix with electrochemically in-house synthesized few layer graphene nano-sheets as reinforcement. *J. Alloys Compd.* **2018**, *750*, 587–598. [CrossRef]
34. Rosa-Ortiz, S.M.; Khorramshahi, F.; Takshi, A. Study the impact of $CuSO_4$ and H_2SO_4 concentrations on lateral growth of hydrogen evolution assisted copper electroplating. *J. Appl. Electrochem.* **2019**, *49*, 1203–1210. [CrossRef]
35. Saeki, I.; Harada, T.; Tanaka, I.; Ando, T.; Gan, L.; Murakami, H. Electroplating of Copper on Low Carbon Steel from Alkaline Citrate Complex Baths. *ISIJ Int.* **2020**, *60*, 2031–2037. [CrossRef]
36. Ge, Y.C.; Zhu, Z.W.; Wang, D.Y. Electrochemical Dissolution Behavior of the Nickel-Based Cast Superalloy K423A in $NaNO_3$ Solution. *Electrochim. Acta* **2017**, *253*, 379–389. [CrossRef]
37. Liu, Y.; Qu, N.S. Electrochemical Milling of TB6 Titanium Alloy in $NaNO_3$ Solution. *J. Electrochem. Soc.* **2019**, *166*, E35–E49. [CrossRef]
38. Berthe, L.; Fabbro, R.; Peyre, P.; Tollier, L.; Bartnicki, E. Shock waves from a water-confined laser-generated plasma. *J. Appl. Phys.* **1997**, *82*, 2826–2832. [CrossRef]
39. Itina, T.E. On Nanoparticle Formation by Laser Ablation in Liquids. *J. Phys. Chem. C* **2011**, *115*, 5044–5048. [CrossRef]
40. Wang, Q.S.; Jiang, L.; Sun, J.Y.; Pan, C.J.; Han, W.N.; Wang, G.Y.; Zhang, H.; Grigoropoulos, C.P.; Lu, Y.F. Enhancing the expansion of a plasma shockwave by crater-induced laser refocusing in femtosecond laser ablation of fused silica. *Photonics Res.* **2017**, *5*, 488–493. [CrossRef]
41. Nguyen, T.T.P.; Tanabe-Yamagishi, R.; Ito, Y. Impact of liquid layer thickness on the dynamics of nano- to sub-microsecond phenomena of nanosecond pulsed laser ablation in liquid. *Appl. Surf. Sci.* **2019**, *470*, 250–258. [CrossRef]
42. Simakin, A.V.; Voronov, V.V.; Shafeev, G.A. Nanoparticle formation during laser ablation of solids in liquids. *Phys. Wave Phenom.* **2007**, *15*, 218–240. [CrossRef]
43. Sasaki, K. Temporally-Resolved Measurements on Growth Processes of Nanoparticles in Laser Ablation. *Rev. Laser Eng.* **2010**, *38*, 113–119. [CrossRef]
44. Soliman, W.; Takada, N.; Sasaki, K. Growth Processes of Nanoparticles in Liquid-Phase Laser Ablation Studied by Laser-Light Scattering. *Appl. Phys. Express* **2010**, *3*, 3. [CrossRef]

45. Bashkatov, A.; Genina, E. Water refractive index in dependence on temperature and wavelength: A simple approximation. *Proc. SPIE Int. Soc. Opt. Eng.* **2003**, *5068*. [CrossRef]
46. Otipka, P.; Vlček, J.; Lesnak, M.; Talík, A. Designing of refractive index of NaCl solution using SPR. *Proc. SPIE* **2008**, *4*, 374–379. [CrossRef]
47. Fujiwara, S.; Nishimoto, Y.; Arakawa, F. Fluctuation of Refractive Index of Aqueous Sodium Chloride Solution and Oxygen Effect. *Anal. Sci.* **1985**, *1*, 23–27. [CrossRef]
48. Graber, T.A.; Taboada, M.E.; Cartón, A.; Bolado, S. Liquid−Liquid Equilibrium of the Poly (ethylene glycol) + Sodium Nitrate + Water System at 298.15 K. *J. Chem. Eng. Data* **2000**, *45*, 182–184. [CrossRef]
49. Mamyrbekova, A.K. Concentration dependences of the density, viscosity, and refraction index of $Cu(NO_3)_2$ $3H_2O$ solutions in DMSO at 298 K. *Russ. J. Phys. Chem. A* **2013**, *87*, 414–417. [CrossRef]
50. Wani, N.V.; Biradar, U.V.; Dongarge, S.M. Refractive Index of Copper Sulfate Pentahydrate from Aqueous Solution. *Int. J. Phys. Appl.* **2017**, *9*, 11–18.
51. Kodama, S.; Shimada, K.; Mizutani, M.; Kuriyagawa, T. Effects of Pulse Duration and Heat on Laser-Induced Periodic Surface Structures. *Int. J. Autom. Technol.* **2020**, *14*, 552–559. [CrossRef]